Maui4: a 24 hour Haleakala turbulence profile

L. William Bradford

Pacific Defense Solutions, LLC, Kihei, HI

Introduction

Recent research efforts to improve daylight imaging techniques on both the Advanced Electro-Optical System (AEOS) and the Maui Space Surveillance Site (MSSS) 1.6 m telescope have resulted in a need to generate a new daylight and low elevation turbulence model. Previous turbulence models used for Haleakala-based telescopes were not adequate for estimating of r_0 and θ_0 at low elevation and mid-day conditions. For example, the now standard Maui3 model uses a median value of r_0 that is more representative of night-time conditions than of day-time conditions. Research into imaging performance over a broad range of daylight hours and low elevations led to the development of a more versatile turbulence model called the Maui4. This report describes the Maui4 model and the data from which it was constructed.

Background - Maui3 Turbulence Model

A description of the Maui3 turbulence model and its origins is useful in understanding the current development of the Maui4 model. Despite limited measurements, several models specific to Haleakala have been developed over the years.

One of the first models for Haleakala was the Maui Night Model. The model was based on a set of thermosonde measurements made by AFRL in the mid-1980s [1]. Although data was collected during the day and the night, the daytime data was known to be contaminated by intermittent solar heating of the probes. The thermosonde campaign had a relatively small number of measurements, but remains as the best set of direct measurements of C_n^2. Beland reports that the value of r_0 found from the subsequent model was 8.9 cm and the isoplanatic angle θ_0 was 12.4 microradians . *Note that all values of r_0 and θ_0 are reported for a wavelength of 500nm, and for a zenith angle of 0 degrees, unless otherwise noted. Standard scaling laws are used to scale measurements* [1].

In the late 1980s, a set of measurements of r_0 and θ_0 was collected at MSSS using a Hughes developed seeing monitor mounted on the 1.6 m telescope. These measurements produced a median r_0 value of 12.9 cm and 9.6 microradians for θ_0 [2]. In addition, an alternative model by Nahrstedt and Brinkley was briefly used for C_n^2 modeling of active illumination experiments at MSSS[3]. With special consideration given to the four years of seeing monitor data, a new turbulence model based on the original thermosonde data was developed. In particular, the turbulence model was tuned to deliver the median values from the four years of seeing monitor data. A ground layer portion of the turbulence model was also based on the Nahrstedt-Brinkley model with inputs from R. B. Holmes [4].

The resulting model was initially called the Median Parameters model, but it was later renamed to Maui3 to follow a nomenclature used by Holmes. Maui3 became the standard for use in the analysis of Maui-based experiments including the Maui Active Track Program. Results from Maui3 including r_0, θ_0, and scintillation phase variance σ_χ^2 were consistent with results obtained from a turbulence model independently developed by G. A. Tyler. Profiles of the AMOS Night Model and Maui3 C_n^2 as a function of altitude above sea level are shown in Figure 1.

The AMOS Night Model (Beland, 1993) is described by the following equations where the variable z is the altitude above sea level.

For an altitude greater than 3.052 km but less than or equal to 5.2 km:

$$C_n^2(z) = 10^{-12.412-0.4713z-0.0906z^2}$$

For an altitude greater than 5.2 km but less than or equal to 30 km:

$$C_n^2(z) = 10^{-17.1273-0.0301z-0.0010z^2+0.5061exp\left\{-0.5\left[\frac{z-15.0866}{3.2977}\right]^2\right\}}$$

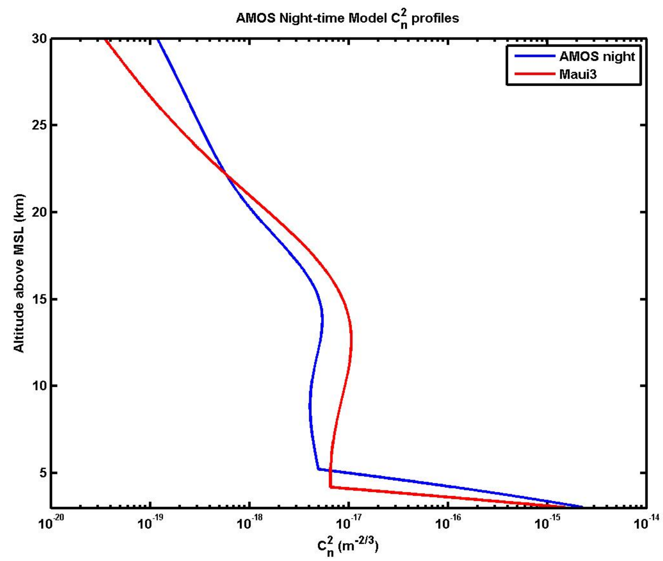

Figure 1. C_n^2 vs altitude above Mean Sea Level from the AMOS Night Model and the Maui3 model.

The Maui3 model is described by the following equations where z also represents the altitude above sea level.

For an altitude greater than 3.05 km but less than or equal to 4.2 km:

$$C_n^2(z) = 10^{-9.4010-1.5913z-0.0606z^2}$$

For an altitude greater than 4.2 km but less than or equal to 25 km:

$$C_n^2(z) = 10^{-17.1273-0.0332z-0.0015z^2+0.9061exp\left\{-0.5\left[\frac{z-15.0866}{5.2977}\right]^2\right\}}$$

Furthermore, above 25 km, the latter profile is modified by a factor of:

$$e^{-\frac{z-25}{5}}$$

This term was added to reduce the higher level values of C_n^2 to values similar to other measurements by different thermosonde probes and has only minor impact on calculations. However, one clearly sees that Maui3 was derived from the AMOS Night Model. The development was iterative, based on first matching isoplanatic angle and then r_0, then iterating until a match to the two desired numbers was achieved. Note that while the changes to the upper portion of the profile seem small, this is belied by Figure 1.

By 2006 data from the University of Hawaii's Day-Night Seeing Monitor (DNSM) on Haleakala and from long exposure images taken on the AEOS Visible Imager camera, showed that the median night-time value of r_0 was better (14.7 cm) than what Maui3 predicted [5]. The DNSM data also showed a median value of 9.7 cm for daytime r_0s. However, because there was less than 3 years of data from the DNSM, and a limited number of AEOS Visible Imager images were available, no change was made to Maui3.

A Daylight, Low Elevation Turbulence Model

During the daytime and at low elevation angles, the median hourly variation in r_0 becomes significant and the single value models like Maui3 and HV5/7, have limited utility. These limitations led to development of the Maui4 turbulence model. Maui4 uses Maui3 as a basis for the basic C_n^2 profile, but with an adjustment to the boundary layer to account for diurnal variations in r_0. Recent work by Roadcap and Tracy indicates that there may not be large differences between night and day profiles above the atmospheric boundary layer [6].

As a starting point to developing the Maui4 turbulence model 854,000 DNSM measurements (262,000 day and 592,000 night) collected between 2002 and 2009 were analyzed. For this data, the median nighttime r_0 is 14.9 cm and the median daytime r_0 is 10.2 cm. The latter value is not truly representative, because the statistics are dominated by measurements made in early morning or late afternoon, when r_0 is larger. Data reported by the Advanced Technology Solar Telescope site survey provided the basis for modeling the turbulence profile nearest the surface [7].

A thorough description of the DNSM and ATST data will help the reader understand methodology to the Maui4 development. These descriptions are provided now.

The Day Night Seeing Monitor

The UH DNSM is a 40cm diameter telescope on a tower at the Zodiacal Light Observatory (Figures 2) [8]. The DNSM rides an elevator up to its observing position, but is stowed during inclement weather. The location and approximate 10m height of the tower act to make the measurements relatively free of orographic and dome effects that affect the telescopes in the older MSSS building. The AEOS telescope is similarly located above a significant part of the surface layer turbulence [9].

The DNSM uses the principle of differential image motion to compare the motion on the focal plane of the images formed by 4 circular apertures on the telescope entrance pupil [10]. A varying number of images (100-450), taken at 200 fps are used to create a single measurement. The root-mean-square (rms) image shifts are converted to a value of r_0 by interpolating against a set of reference equations relating apparent wavefront tilt and image intensity to r_0 [8].

Bright stars are used for the observation, with most observations above 45 degrees. A daily list of objects is prepared beforehand, and is available from http://banana.ifa.hawaii.edu along with measurements of the seeing. The list of available stars includes all stars brighter than 3rd magnitude which fall within the pointing limits of the telescope, constrained to be roughly +/- 23 degrees declination and 3 hours above the horizon. These restrictions are the result of telescope mount limitations as it was originally constructed as a solar telescope. The overall result is that the target stars must at any time lie within a roughly rectangular area, approximately 46 degrees North-South by 90 degrees East-West, centered on the celestial equator and the meridian.

During the day a red filter is used to reduce scattered light, but this filter may also be in place at night. The blue end of the filter cuts off at about 600 nm. Since the system is optimized for performance in the R and I bands, this does not affect night-time performance. When they are reported, all r_0 values are scaled to 500nm. The DNSM does not adjust for the zenith angle, but all data reported here has been so adjusted. The DNSM is not usually operated in the hours near local noon to prevent damage to a tracking sensor.

Weather data (pressure, humidity, temperature, wind speed & direction, etc.) is also recorded with each r_0 measurement from instruments located on the same tower as the DNSM.

Figure 2. The UH DNSM is housed in the tower on the right. Weather instruments are visible.

Distribution and Exceedance of r_0 from Sunrise to Sunset

In the process of analyzing the DNSM data numerous plots were generated. These include distribution of measurements versus time of day, by season and wind speed. However, a number of plots are useful in showing how the data influenced the form of the Maui4 model. Figure 3 shows the distribution of r_0 during daylight hours. The times for sunset and sunrise are approximate as monthly average times are used. The times of sunrise and sunset are also adjusted to account for the height of Haleakala.

The distribution is weighted toward higher r_0 values because relatively few measurements are made when the seeing is worst (around local noon) and because the accuracy of the DNSM is reduced for very strong turbulence. Note that there are over 262,000 measurements during the day. The median value of r_0 is 10.2 cm. However, that value is influenced by the distribution of measurements with time, which has many measurements early in the morning and later in the afternoon and few during the mid-day.

Figure 4 shows the probability of "exceedance" which is calculated as 1 minus the cumulative distribution function. The plots should be interpreted as showing that the probability that a value of r_0 (horizontal axis) will be exceeded (by measured data) is given by the value on the vertical axis.

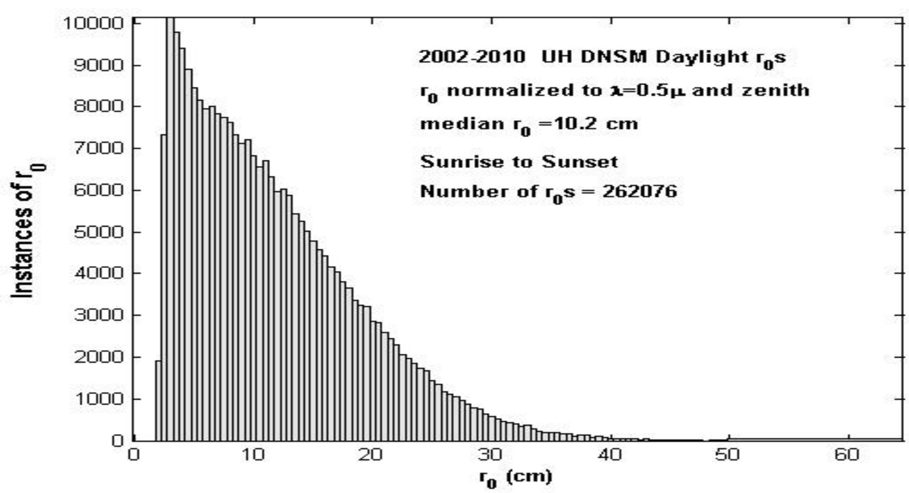

Figure 3. Distribution of r_0 measured from local sunrise to local sunset.

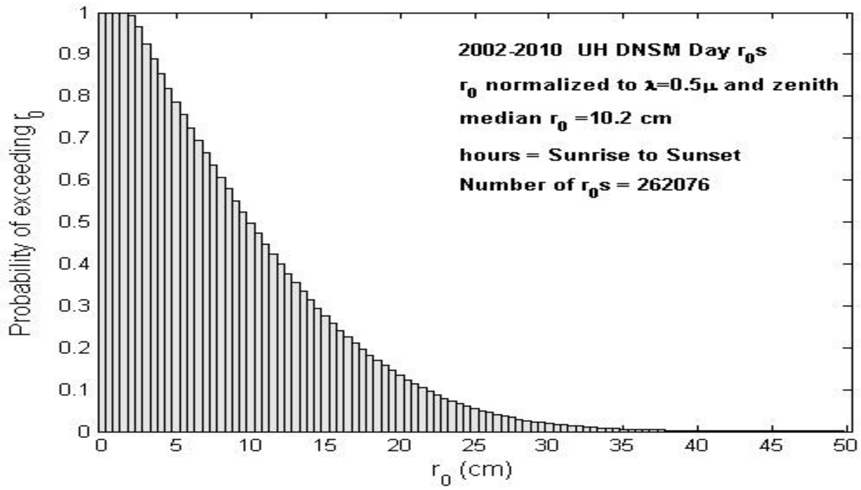

Figure 4. Exceedance Plot for Daytime Data.
Vertical axis shows the fraction of measurements of r_0 that exceed a particular value of r_0

Distribution and exceedance of r_0 from sunset to sunrise

Figure 5 shows the distribution of r_0 from local sunset to local sunrise. The distribution is again likely weighted toward higher r_0 values due to fewer measurements made during poor conditions. Because this is a sporadic effect, as opposed to the systematic omission of measurements at local noon, it is not a large effect. Moreover, most of the time omissions will correspond to conditions when observations with other telescopes are also limited. Figure 6 shows the probability of r_0 exceeding a given value, as before. Some rather high r_0 values are shown, but other measurements also show some fairly large r_0 values.

For the nighttime data the median value is 14.9 cm, while the median value for Maui3 measurements was 12.9 cm. This represents a significant improvement in seeing and can be partly attributed to the sites of the two seeing monitors being different. The seeing monitor whose data was used for Maui3 was located on the 1.6 m telescope. During site testing for the AEOS telescope, it was found that a significant surface layer was present at the site, which led to the recommendation that AEOS be located where it is, and also that it be elevated [9]. The UH DNSM is elevated above the MSSS site, so it can be expected to have better seeing. Differences in the seeing monitors may be a factor, but a lack of documented information for the earlier seeing monitor precludes comparative analysis. However, several thousand long exposure (0.5 to 2 seconds) measurements at AEOS, using the Visible Imager camera and taken over an extended period of time, gave a median r_0 of about 14.6 cm. These results, which are shown in Figures 7 and 8, increase confidence in the DNSM night-time measurements. The reader should note that a few values of r_0 in the range of 50 cm are shown. This lends credence to the larger DNSM values noted above.

Hourly distribution of r_0 data

While the previous distributions show differences in the day and night median values, there is significant variation in the median value of r_0 from one hour to the next, so that use of the median values for the entire day or night can be misleading. Figure 9 is a histogram showing how the values are distributed each hour of the day. The darker shading corresponds to larger r_0 values. The 13:00 HST period is blank because no significant amount of data has been acquired at that time. The plot shows that at 7:00 HST more than 75% of the r_0 measurements exceed 10cm. Yet at 8:00 HST only 50% exceed 10 cm, and at 14:00 HST 60% of the measured r_0 are less than 5 cm. This large variation led to the approach of modeling the turbulence using a time of day dependent C_n^2 model for daytime imaging.

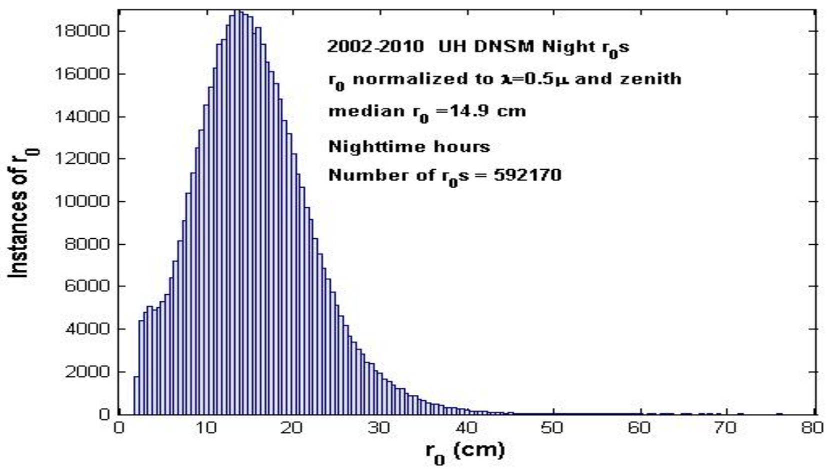

Figure 5. Distribution of r_0 measured from local sunset to local sunrise

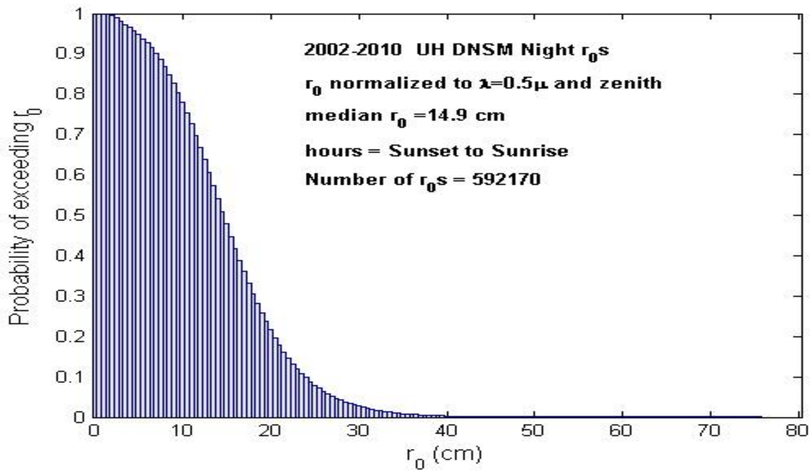

Figure 6. Exceedance Plot for Nighttime Data
Vertical axis shows the fraction of measurements of r_0 that exceed a particular value of r0

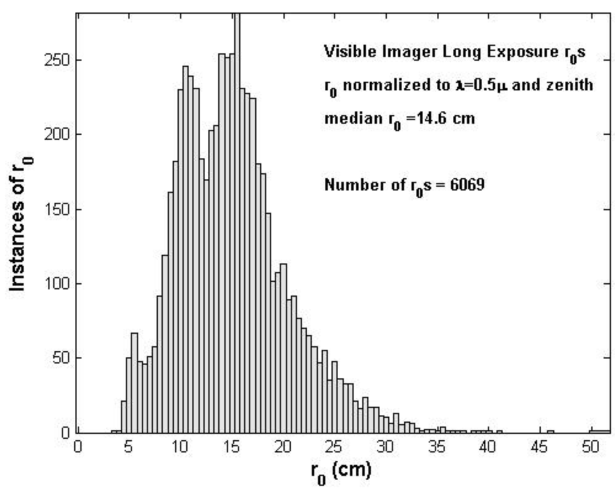

Figure 7. Distribution of r_0s from long exposure (0.5s to 2s) Visible Imager images of stars.

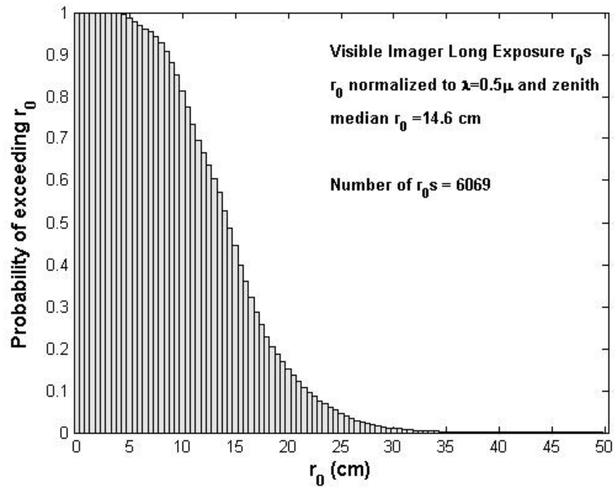

Figure 8. Exceedance Plot for Visible Imager r_0 data

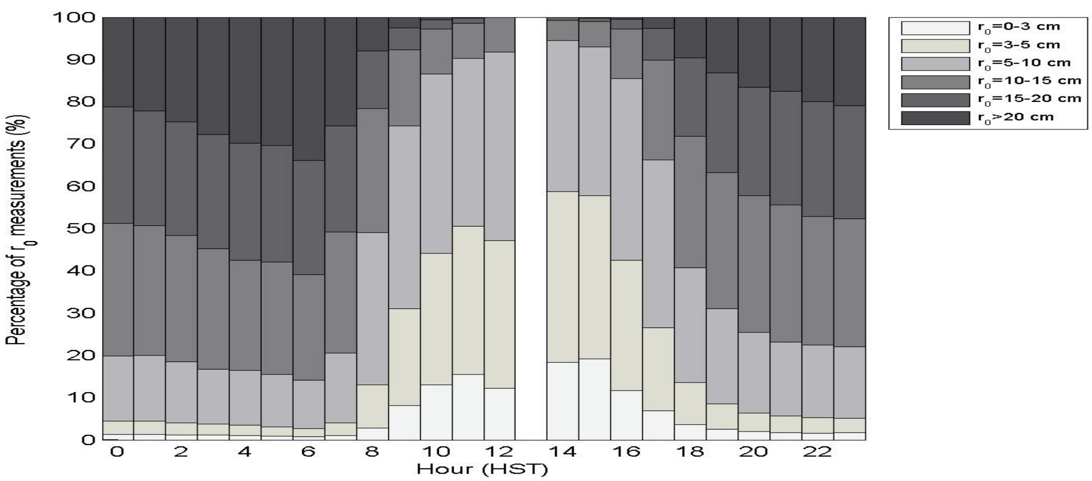

Figure 9. Distribution of ranges of r_0 by hour

Figure 10 shows the measured statistics of r_0 by the hour while figure 13 shows the number of r_0 measurements made during each hour. There is an appreciable spread of values at any hour. The error bars are +/- 1 standard deviation from the mean value for the hour. Note that the means are larger than the medians, because the distributions have a relatively long tail. Figure 11 shows that the measurements during the hours near noon are relatively sparse. This means that taking a mean or median value of all the daytime r_0 yields a result weighted toward hours which have higher values of r_0. If, for example, we treat each hourly median value as having equal weight, the median daytime value would be 5.5 cm. The hourly medians are calculated without taking into account whether the data was measured before or after sunrise or sunset. Nevertheless, it is clear that there is considerably more variation in the median values during the day than during the night.

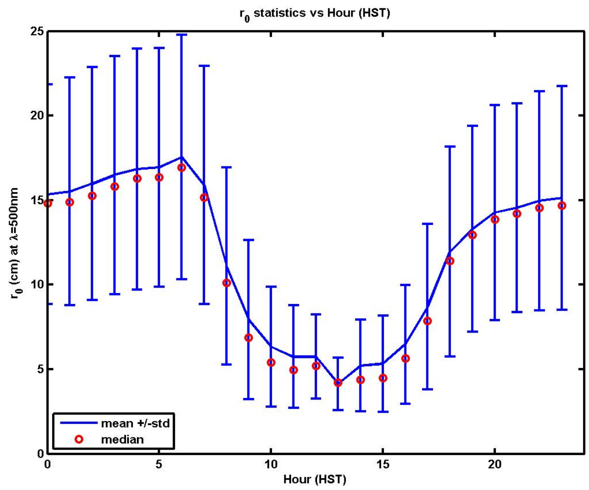

Figure 10. Red circles indicate the median r_0 during that hour. Solid curve shows the mean, and error bars are +/- one standard deviation.

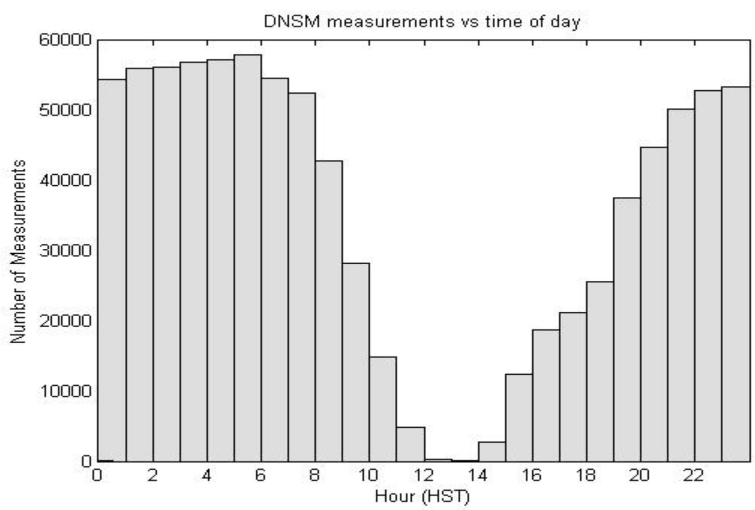

Figure 11. The number of r_0 measurements during each hour is shown.

Distribution of DNSM data with zenith angle

Earlier it was mentioned that the DNSM monitor did not operate over all zenith angles. In addition to the limitations imposed by the DNSM telescope mount described earlier, there is a need to have relatively bright stars for sources. This will be especially true during daytime. As one looks at lower elevation angles, the signal to noise ratio of the DNSM is expected to decrease because of the longer path through the atmosphere. For all these reasons, one expects most measurements to be made with zenith angles less than 45 degrees.

Wind and r_0

While the development of the Maui4 model does not depend on the surface wind, the data shows that there is some correlation between smaller r_0 and increasing surface wind speed. There is a mild correlation with the wind direction, but this may simply be because of the frequency with which the wind is from the east. The distribution of r_0 when the winds are calm is also shown. The median r_0 is found to be 16.3 cm in data that has not been sorted into day and night regimes.

Variations in the distributions with season

In addition to varying hourly, one finds that there are seasonal variations in the data as wellTable 1 summarizes the median r_0 values by season.

	Day	Night
Spring	**10.1**	**15.3**
Summer	**9.4**	**13.5**
Fall	**11.3**	**14.9**
Winter	**10.3**	**16.6**

Table 1 Median r_0 values (cm) by season

The Atmospheric Boundary Layer

Observation of Figure 1 shows that a significant difference in the Maui3 and AMOS night model occurs in the lower portion of the curves. This represents an attempt to model the behavior of C_n^2 in the atmospheric boundary layer. Over the continents, and over flat terrain, the depth of the atmospheric boundary layer ranges from about 300m at the most quiet part of the night to a kilometer or more during the afternoon [11]. The height is subject to variation from wind and clouds. Figure 12 illustrates the structure and dynamics of the boundary layer.

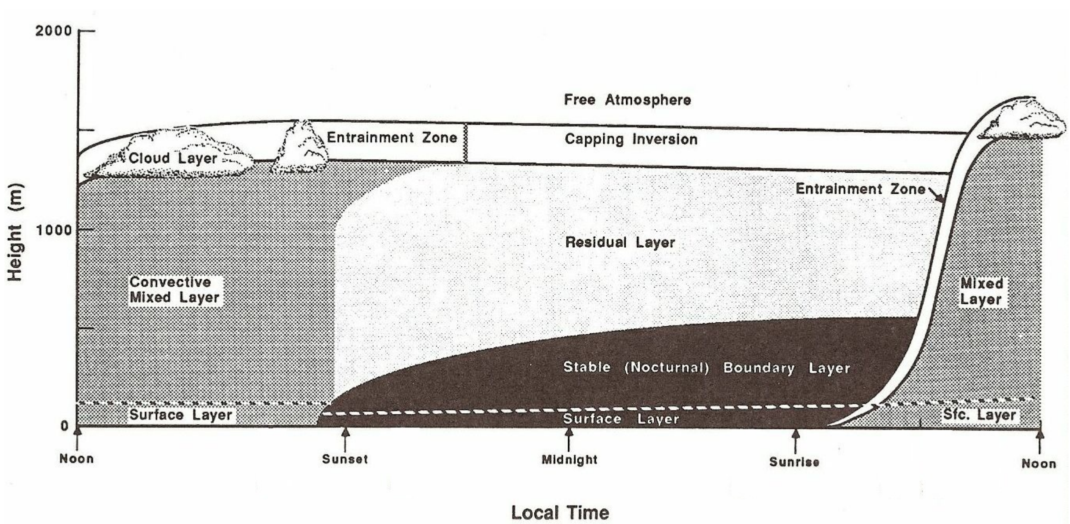

Figure 12. A schematic view of the components of the atmospheric boundary layer. Heights are notional. During the day, in some locations, the height can be anywhere from 1 to 2 km. The important point to this figure is that the boundary layer varies throughout the day. From R. B. Stull, *An Introduction to Boundary Layer Meteorology*, Kluwer Academic Publishers, 1988.

The important thing to notice about Figure 12 is that the boundary layer changes significantly during a diurnal period. This obviously reflects the absorption and re-radiation of energy by the ground during the day leading to convective motion of the air. At night, the ground has generally cooled off faster than the air, so that air near the surface is more stable than during the day, leading to the formation of the nocturnal boundary layer. As one goes higher than the capping inversion layer (at 1 to 2 km above the surface), the turbulence in the free atmosphere is much less affected by the solar heating, and so it is expected that the diurnal variation of the free atmosphere will be much less than that of the boundary layer.

Recent thermosonde data that shows for a few continental measurements, that the variation of the upper level C_n^2 profiles is not great [6]. For Hawaii, where the surface is uniformly ocean for thousands of miles, one would expect fewer possible forces to disturb the upper part of the air, at least on average.

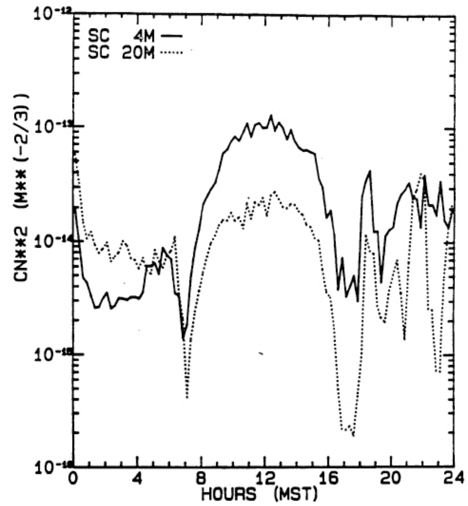

Figure 13. Diurnal variation of C_n^2 at 4 and 20 meters above the surface at a site in New Mexico. From F. D. Eaton, *et al., Optical Turbulence at Kitt Peak National Observatory, Fred Whipple Observatory, Apache Peak Observatory, Horace Mesa, and the Atmospheric Profiler Research Facility*, Army Research Laboratory Report, ARL-TR-1013, June, 1996

That is not the case for the boundary layer. There is an abundance of measurements of C_n^2 profiles in the diurnal cycle. One such set is shown in Figure 13[12]. The particular data here represent measurements along horizontal paths at 4 meters and 20 meters above the surface using a scintillometer. As can be seen, the turbulence strength at 20 meters is nearly an order of magnitude less than at 4 meters. This decrease with height is not unique to this set and has been noted in other publications [13]. Another feature in the diurnal variation is the drop in C_n^2 at dawn and sunset. Particularly on Haleakala, dawn seems to offer the best seeing during the day. The difference between 4 and 20 meters is also why AEOS is set as high as it is [9]. The location of the UH DNSM in a tower also means that it too is at a relatively favorable height.

More significant to building a diurnal model of the turbulence is the fact that from sunrise to noon, C_n^2 varies by nearly two orders of magnitude near the surface. This suggests that most of the variation of r_0 during the day is indeed due to the boundary layer variations of C_n^2. Figure 12 indicates the fact that the boundary layer thickness changes during the day and night. These variations are difficult to capture in any analytic manner, and vary with winds, etc.

Advanced Technology Solar Telescope measurements

During the years leading up to the selection of Haleakala as the site for the Advanced Solar Technology Telescope, site tests were conducted to evaluate seeing at several locations. The results are detailed in a final report [6].

Part of the effort used a scintillometer array that could accurately evaluate C_n^2 over the first 100 meters that Rimmele wrote could make “a reasonable estimate for heights between 100-500m” [14]. Rimmele used this data to select two profiles which he said corresponded to r_0 of 7cm and 12 cm.. Rimmele then merged these profiles with profiles from Mauna Kea, supposing that above a certain altitude, the profiles should be similar for Haleakala and for Mauna Kea. This is plausible, but not certain.

Figure 14 shows three plots of C_n^2 from Rimmele’s report. The range of heights is less than a meter above the surface to more than 100 meters. The surface values shown for the 7cm and 12 cm are about two orders of magnitude larger than the surface value of Maui3, but that is a night model. The surface values shown are similar to values reported elsewhere, including Beland [1]. The data also supports the idea of having telescopes elevated 10-20 meters above the surface.

As mentioned above, the next step in Rimmele's analysis was to use two profiles from Mauna Kea and merge the two low level profiles with those. The result is shown in Figure 15. The SCIDAR profiles, based on this author's experience do not look unreasonable. Real profile data tends to have multiple peaks just as shown. So separately these all look good. And when merged, the results still look reasonable. However, this author digitized the plots and integrated the C_n^2 profiles, which led to the result that the "7 cm" profile had an r_0 of 2.93 cm, while the "12 cm" profile yielded an r_0 of 2.30 cm. That result nearly ended any attempt to make use of the data from ATST.

However, a re-examination of the data showed that the initial height of the data sets (as digitized) were 2997 meters and 3008 meters respectively. The data was interpolated for altitudes from 3010 to 24800 meters. Then only data from heights greater than 3050 meters (the base height for Maui3) were used. With this interpolated data, both profiles yielded an r_0 of 7.03cm.

The above results were a little puzzling so that the utility of Rimmele's curves was in doubt. But the ATST final report offers some other curves, amongst them an "average C_n^2 profile" for Haleakala [6]. This data was digitized and is shown in Figure 16, along with a simple model curve that follows the data at least for a while. Given that Rimmele has remarked that the first 100 meters are so are the best data, divergences at scales of a kilometer or more are probably irrelevant. In fact, an earlier version of a fit to the ATST curve was better at the higher altitudes, but that fit was dropped, because emphasis shifted to altitudes less than 100 meters.

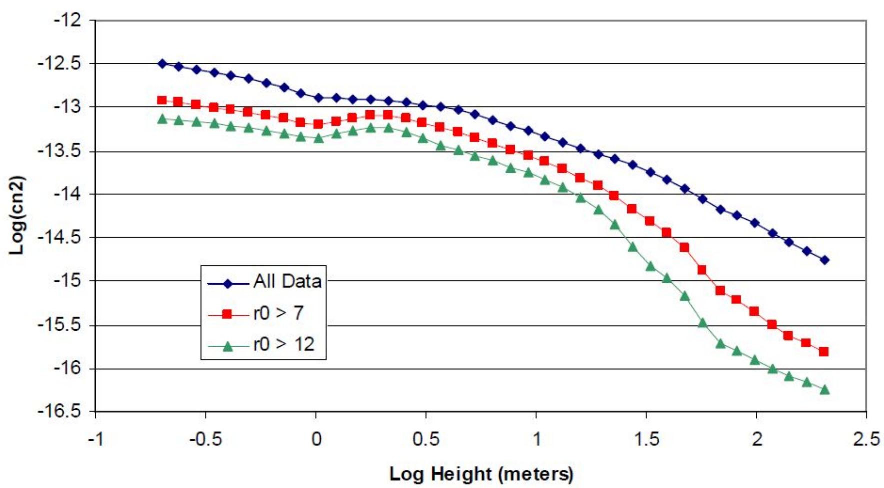

Figure 14. C_n^2 profiles as reported by Rimmele. Note the strong values near the surface. Telescopes will generally be above such strong values.

Another issue is that the ATST data was collected in the daytime, and Maui3 is night-time data. In Figure 16, a scaling down of the ATST C_n^2 by two orders of magnitude might represent a good match to a night-time profile. But otherwise the profile fails to match with the atmosphere above the boundary layer. For example, the profile above is still an order of magnitude higher than the Maui3 model value at 5 km above the surface. A positive feature, however, is that the profile decreases much more rapidly near the surface than does the Maui3 model. This suggests that a profile which follows this behavior near the surface, but which falls off faster at higher altitudes is to be sought.

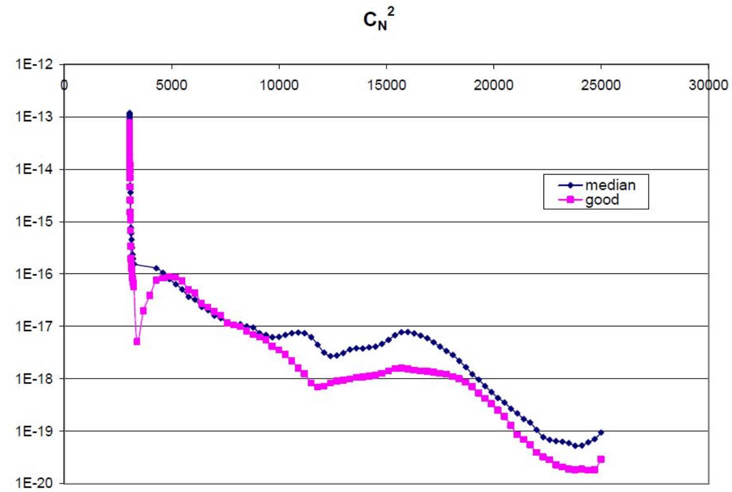

Figure 15. Rimmele's C_n^2 profiles. Median is the "7 cm" profile.

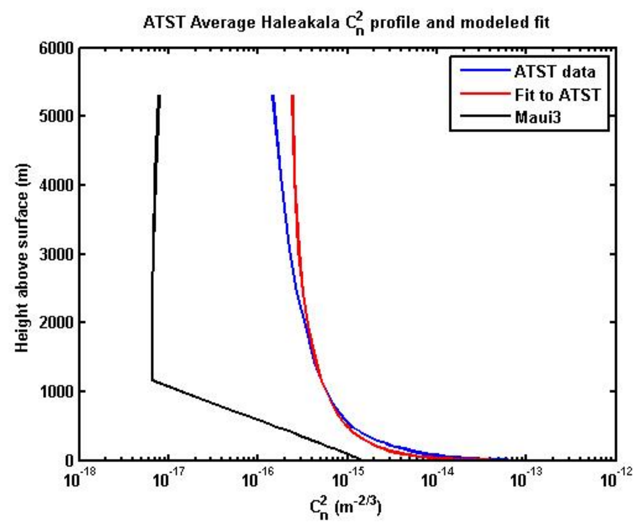

Figure 16. Data digitized from the ATST average Haleakala profile (blue), a simple fit to the data, and the Maui3 model profile.

Some different ways of creating a surface layer term, which would work with the existing Maui3 boundary layer term (the lower part of the Maui3 curve in Figure 16) were tried, but rejected. At that point, an examination of a paper that discussed turbulence modeling in the boundary layer and the free atmosphere using data from instrumented balloons provided a key insight [15]. Several figures in that paper show C_n^2 profiles from the surface to about a kilometer. On the whole, they look similar to the ATST curve. This inspired a renewed effort to find a model fit of the ATST profile.

A two layer model with the upper (free atmosphere) part given by the upper portion of the Maui3 profile, and a lower portion using a modified fit of the ATST data was created. Because that ATST profile became asymptotic to a particular value of C_n^2, as shown in Figure 18, the initial fit was multiplied by a decaying exponential. Through an iterative process, the scale length for the exponential was established at 450 meters. The only other free parameter is the value of C_n^2 at the surface. This was adjusted to match the median hourly r_0 values as measured from a height of 10 meters, the height at which the DNSM is recorded. While some of these surface values are somewhat higher than one would expect from the *mean* ATST data, the surface values used are entirely reasonable for ground level measurements.

In Figure 17, C_n^2 profiles from the Maui4 model for 3 different hours are shown with the Maui3 profile. So that the behavior of the boundary layer term can be seen more clearly, only the first 2500 meters above the surface are shown.

The time 23:00 UT corresponds to the smallest median hourly r_0, while 16:00 UT corresponds to the largest median hourly r_0. The profile for 5:00 UT is included because the corresponding r_0 is the nearest to the value for Maui3. A feature to note is that when the value of C_n^2 at some height as computed for the boundary layer falls below the value of the free atmosphere term, then the latter is used. This means that the intersection point (which effectively marks the end of the atmospheric boundary layer in the model) slides up and down during the diurnal period. This mimics the daily variation of the thickness of the real atmospheric boundary layer.

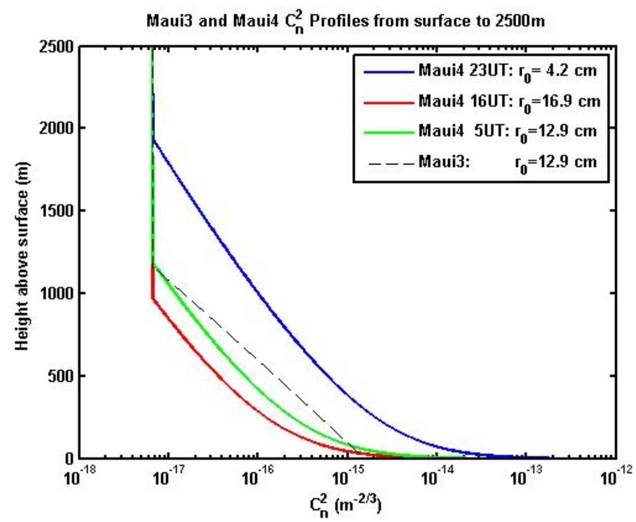

Figure 17. Behavior of Maui3 and three select Maui4 profiles in the atmospheric boundary layer.

It may be that the Maui3/Maui4 models do not have precisely the correct profiles for the lower section of the atmosphere. But there is not enough information to say precisely how Maui4 might be improved. We do know that the telescopes, particularly AEOS are high enough to avoid the worst of the ground level turbulence. The current form of the Maui4 model gives profiles that mimic that behavior.

The best way to determine what changes might be needed is to measure. A radar sounder could probe the first 3km above the surface, and give some high resolution data. Acoustic sounders would be perhaps even more limited than the ATST scintillometer in altitude range. Generalized scintillation detection and ranging (SCIDAR) would provide profiling information, but only at relatively large vertical intervals [16]. And for best results, AEOS should be used with fairly bright, well separated double stars which would limit the number of measurements. It might be useful to look into a scintillometer array such as that used for ATST, used with the sun during the day, and at night with the moon. This would be in addition to any other methods used to measure r_0, such as the DNSM.

The Maui4 model

As noted in the introduction, the Maui3 model was based primarily on measured C_n^2 profiles. To develop the Maui3, those profiles were adjusted to fit additional measurements, which represented not only measurements of the integrated profile (r_0) but of an altitude weighted integration (θ_0). If data reflecting the altitude variation (either isoplanatic angle θ_0 or scintillation index σ_χ^2) was available, the entire C_n^2 profile could be refined. However, the UH DNSM provides only r_0, so there is no other new knowledge available for the Maui4 turbulence model development.

Typically modelers will simply multiply an entire C_n^2 profile to obtain a particular value of r_0. However, for a diurnal variation, for which the Maui4 model is designed, this was considered unphysical. Instead the Maui4 model was built upon the premise that the diurnal variations reflected an intensification of turbulence in the atmospheric boundary layer. Earlier, the boundary layer portion of the Maui3 model was described by the following.

For an altitude above sea level greater than 3.05 km but less than or equal to 4.2 km:

$$C_n^2(z) = 10^{-9.4010-1.5913z-0.0606z^2}$$

For Maui4, the form for the boundary layer profile of $C_n^2(z,h)$ is valid in the altitude range from 3.05 km to 5.7 km above sea level. Below 3.05 km, C_n^2 for both Maui4 and Maui3 is zero.

$$C_n^2(z,h) = \frac{0.2290\times a(h) \times e^{-\frac{z-3.05}{0.450}}}{[0.13 + 0.1\max((z-3.05)*1000,1) - 0.001(\max((z-3.05)*1000,1))^{4/3}]}$$

Where *z* is height in km above the surface and *h* is the hour of the day. The effect of the expression *max*((*z*-3.05)*1000,1) is to set the value of the denominator at the surface (3050m ASL) to be the same as the value at 1 meter above the surface (3051m ASL). This form arose from a more or less arbitrary decision made during model development.

It should be noted that the values of *a (h)* were obtained by an integration of the entire profile from the surface to 30 km using 1 meter increments in altitude and iterating until the desired value of r_0 (the median for the hour) was obtained. A choice of a different increment or upper bound will lead to a slightly different value for the computed r_0.

While the form of the equation above is specified to be from z=3.05 km to 5.7 km, the height over which the lower term is applicable will vary. In code, for the range of values of z from 3.05 km to 5.7 km, the value of C_n^2 from the above equation is compared against the value of C_n^2 calculated using the profile for the upper atmosphere portion of the Maui3 model (which is the same for Maui4), and the largest C_n^2 value is used. The effect of this can be seen in Figure 17, where the lower profiles intersect the Maui3 profile at different altitudes. This assures that there are no discontinuities in the combined profile.

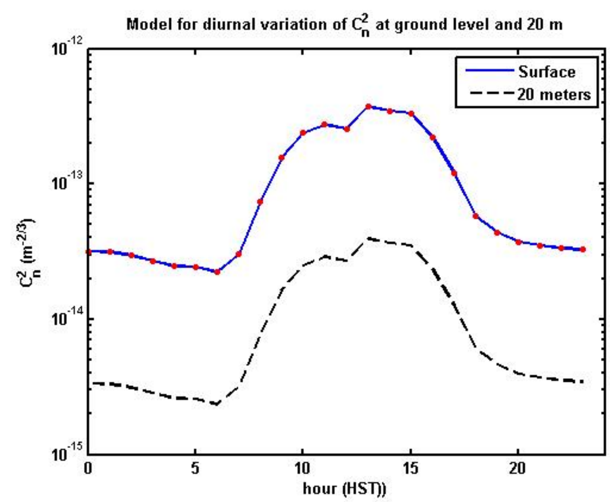

Figure 18. Diurnal variation of of C_n^2 at the surface and 20 meters above the surface using the Maui4 model. The red dots indicate the surface values of C_n^2.

As a check on the model's fidelity, in Figure 18 the value of C_n^2 at the surface and at 20 meters above the surface from the Maui4 model is plotted against the time of day. Some resemblance to Figure 13 is to be expected, but Figure 18 represents data which has been averaged over an hour instead of a few minutes, and furthermore is an average over thousands of days. So only a general agreement is to be expected. In this case, the deep decrease in C_n^2 at sunrise and sunset is lost.

Hour of the day (UT)	Number of measurements	mean r_0 (cm)	standard deviation (cm)	median r_0 (cm)	*a(hour)* $m^{-2/3}$
0	2646	5.2045	2.7118	4.3819	$3.4589\cdot10^{-13}$
1	12359	5.3219	2.8569	4.4892	$3.3162\cdot10^{-13}$
2	18719	6.4744	3.5160	5.6387	$2.2199\cdot10^{-13}$
3	21139	8.6886	4.8983	7.8560	$1.2120\cdot10^{-13}$
4	25612	11.964	6.2058	11.4229	$5.7698\cdot10^{-14}$
5	37374	13.287	6.0859	12.9495	$4.3834\cdot10^{-14}$
6	44620	14.266	6.3600	13.8480	$3.75185\cdot10^{-14}$
7	50080	14.547	6.1816	14.2177	$3.5223\cdot10^{-14}$
8	52701	14.964	6.4755	14.5336	$3.3383\cdot10^{-14}$
9	53269	15.13	6.6077	14.6675	$3.26345\cdot10^{-14}$
10	54377	15.341	6.4929	14.8207	$3.1800\cdot10^{-14}$
11	55914	15.515	6.7447	14.8946	$3.1406\cdot10^{-14}$
12	56060	15.971	6.8962	15.2671	$2.9494\cdot10^{-14}$
13	56670	16.483	7.0358	15.8093	$2.69225\cdot10^{-14}$
14	57055	16.839	7.1337	16.3000	$2.47875\cdot10^{-14}$
15	57784	16.944	7.0579	16.3433	$2.4524\cdot10^{-14}$
16	54533	17.545	7.2422	16.9198	$2.23215\cdot10^{-14}$
17	52385	15.89	7.0315	15.1508	$3.00775\cdot10^{-14}$
18	42633	11.107	5.8269	10.1211	$7.4095\cdot10^{-14}$
19	28137	7.9345	4.6995	6.8615	$1.55775\cdot10^{-13}$
20	14990	6.3234	3.5444	5.4219	$2.3081\cdot10^{-13}$
21	4900	5.7385	3.0404	4.9662	$2.7498\cdot10^{-13}$
22	280	5.7464	2.4837	5.2120	$2.5523\cdot10^{-13}$
23	9	4.132	1.5591	4.2089	$3.70955\cdot10^{-13}$

Table 2 Statistics of hourly r_0 from UH DNSM and the scaling parameter *a*(hour) used to adjust the boundary layer C_n^2 value at the surface to match the median r_0

Model C_n^2 profile	Atmospheric Region	Height range (km ASL)	Depends on time of day	Equation for C_n^2 as a function of altitude above sea level *z*, where *z* is in km.
Maui3	Boundary Layer	3.05 to 4.2	No	$10^{-9.4010-1.5913z-0.0606z^2}$
Maui3	Free Atmosphere	4.2 to 25	No	$10^{-17.1273-0.0332z-0.0015z^2+0.9061exp\left\{-0.5\left[\frac{z-15.0866}{5.2977}\right]^2\right\}}$
Maui3	Free Atmosphere	25 and above	No	$e^{-\frac{z-25}{5}}\times 10^{-17.1273-0.0332z-0.0015z^2+0.9061exp\left\{-0.5\left[\frac{z-15.0866}{5.2977}\right]^2\right\}}$
Maui4	Boundary Layer	>=3.05 & <5.7*	Yes	$\frac{0.2290\times a(h)\times e^{-\frac{z-3.05}{0.450}}}{[0.13+0.1\max((z-3.05)*1000,1)-0.001(\max((z-3.05)*1000,1))^{4/3}]}$
Maui4	Free Atmosphere	>3.05* to 25	Yes	$10^{-17.1273-0.0332z-0.0015z^2+0.9061exp\left\{-0.5\left[\frac{z-15.0866}{5.2977}\right]^2\right\}}$
Maui4	Free Atmosphere	25 and above	No	$e^{-\frac{z-25}{5}}\times 10^{-17.1273-0.0332z-0.0015z^2+0.9061exp\left\{-0.5\left[\frac{z-15.0866}{5.2977}\right]^2\right\}}$

Table 3 Summary descriptions of the Maui3 and Maui4 profiles. See Table 2 for *a(h).* Below 3.05 km C_n^2 is set to zero.

***Between 3.05 km and 5.7 km ASL, the C_n^2 values from the boundary layer term and the free atmosphere term are compared at each height. The larger of the two values is used. This results in a time varying height at which a profile switches from boundary layer to free atmosphere.**

Summary

A new model for profiling turbulence at Haleakala has been generated. It has the following features:

1) It uses extensive measured data to create a model with values of r_0 that are based on the hourly median values of the data.

2) It captures the quick fall-off in height of the C_n^2 profile found from earlier measurements, by using a new model profile for the atmospheric boundary layer based in part of another extensive set of measurements.

3) By using the new profile, the model captures the diurnal dynamics of the atmospheric boundary layer in a plausible manner.

4) It gives the modeler an alternative to simple scaling of a fixed profile, a method prone to producing odd and unphysical results.

It must be stressed that while there are some conjectural elements to the model, every attempt has been made to incorporate measured data in a manner that is consistent with our knowledge of the behavior of the atmosphere. It is clear that more data would be useful to refine and validate the model. For example, the shape of the turbulence profile in the ABL is invariant, although the height and strength vary in response to the need to fit the measured r_0 values. Without more data, the validity of this assumption is open to question. The shape of the profile itself is to some degree a forced representation of the ATST profile.

The acquisition of new data has driven the evolution of models of Haleakala turbulence profiles from SLC to Maui Night model to Maui3 to Maui4. To proceed further, we must have more data. This should now include instruments that can give us profiles day and night, at low and at high elevation angles. The need for more day measurements is clear if we examine Figure 13. The paucity of late-morning to early afternoon measurements is apparent. There is some uncertainty as to how bad conditions are at that time, because of the lack of measurements and because the DNSM does not report small values of r_0. If the ATST is built on Maui, it is possible that they will be generating the necessary daytime data. But experience has shown that MSSS is best served by having its own suite of instruments.

Acknowledgments

The author would like to thank J. R. Kuhn of the University of Hawaii for information about the Day-Night Seeing Monitor and its data, and for facilitating access to the data. Thanks also to several members of the PDS staff, R. B. Holmes and H. T. Yura for comments at various stages of this report. Neither the model nor this paper would exist without the support of Kim Luu and Stacie Williams of AFRL Det. 15.

References:

1. Beland, R. R., "*Propagation through Atmospheric Optical Turbulence*," The Infrared & Electro-Optical Systems Handbook, Vol. 2, F.G. Smith, Ed., SPIE Press Bellingham, 1993, URL: http://handle.dtic.mil/100.2/ADA364019
2. Walters, D. L. and L. W. Bradford, "*Measurements of r_0 and θ_0: two decades and 18 sites*," Applied Optics, **36**, 7876-7886, 1997
3. Nahrstedt, D. A. and T. J. Brinkley, "*Analysis of nodding system requirements for satellite radiometry,"* Optical Engineering, **34**, 1743--1748, 1995
4. Bradford, L. W. and R. B. Holmes, "*Maui C_n^2 Profiles,"* Report for Maui Active Track Program, February 21, 2003
5. Bradley, *et. al.,* "*Characterization of Meteorological and Seeing Conditions at Haleakala*," PASP, **118**, 172-182, 2006
6. Roadcap, J.R. and P. Tracy, "*A preliminary comparison of daylight and night C_n^2 profiles measured by thermosonde*," Radio Science, **44,** RS2011, 2009
7. Hill, F., "*ATST Site Survey Working Group Final Report*," ATST Project, Report RPT-0021, Tucson, October 6, 2004, URL: http://atst.nso.edu/files/docs/RPT-0021.pdf
8. Kuhn, J. and M. Waterson, "*AEOS – Haleakala Atmospheric Characterization: Final Technical Status Report,*" Institute for Astronomy, University of Hawaii, 2005 (formerly available from http://banana.ifa.hawaii.edu)
9. Walters, D. L., V. J. Gast, T. S. Mattingly and D. Galarowicz, "*Atmospheric Characterization for the Air Force-Maui 4 m Telescope,*" in Adaptive Optics for Large Telescopes Technical Digest 1992, (Optical Society of America, Washington, D.C., 1992), **19**, 17
10. Fried, D. L., "*Differential angle of arrival: Theory, evaluation, and measurement feasibility*," Radio Science, **10,** 71-76, 1975
11. Stull, Roland B., "*An Introduction to Boundary Layer Meteorology*," Kluwer Academic Publishers, Dordrecht, 1988
12. Eaton, F. D., J. R. Hines, J. J. Drexler and J. Northrup, "*Optical Turbulence at Kitt Peak National Observatory, Fred Whipple Observatory, Apache Peak Observatory, Horace Mesa, and the Atmospheric Profiler Research Facility*," Army Research Laboratory Report, ARL-TR-1013, June, 1996, URL:http://handle.dtic.mil/100.2/ADA296417
13. Wesely, M. L. and E. C. Alcaraz, "*Diurnal Cycles of the Refractive Index Structure Function Constant*," JGR, **78**, 6224-6232, 1973
14. Rimmele, Thomas, "*Haleakala Turbulence and Wind Profiles used for Adaptive Optics Performance Modeling*," ATST Project, Report RPT-0030, Tucson, October 24, 2006, URL: http://atst.nso.edu/files/docs/RPT-0030.pdf
15. Abahamid, *et al.,* "*Optical turbulence modeling in the boundary layer and free atmosphere using instrumented meteorological balloons*," Astronomy & Astrophysics, **416**, 1193-1200, 2004
16. Johnston, R. A., C. Dainty, N.J. Wooder, and R. G. Lane, "*Generalized scintillation detection and ranging results obtained by use of a modified inversion technique*," Applied Optics, **41**, 6768-6772, 2002